



# Effect of Casting Thickness on the Solidification Characteristics and Microstructural Parameters of Near-Eutectic Al-Si Alloy Produced by Ablation Casting Process

Mostafa Arabpour<sup>1</sup> · Seyed Mohammad Ali Boutorabi<sup>2</sup> · Hasan Saghafian<sup>2</sup>

Received: 23 November 2021 / Revised: 19 January 2022 / Accepted: 24 January 2022 / Published online: 16 May 2022  
© ASM International 2022

## Abstract

The role of ablation casting process in the case of different thicknesses of a sloping pattern of a near-eutectic Al-Si alloy was evaluated. The time durations for water spray were selected as 100 and 150 s after pouring melts; in addition, 100 and 150 s were related to the first ablation sample (AB1) and the second ablation sample (AB2), respectively. To this end, 8 thermocouples were located in different thicknesses (4 thermocouples on the casting surface and 4 thermocouples at the casting bottom). The results indicated that the cooling rates of the thermocouples located on the surface were 6.9–43.6 times for AB1 and 4.8–22.8 times for AB2, compared to sand casting (SC). Moreover, the cooling rate of the bottom thermocouple was 1.5–21.9 times for AB1 and 1.3–19.9 times for AB2, compared to SC. Eutectic silicon with a size of about 1  $\mu\text{m}$  was obtained through the AB process, and the secondary dendrite arm spacing was reduced to about 90% compared to SC, especially at the ablated casting center. According to the results, the difference in the time duration of water spray did not have much effect on the cooling rate and microstructure. It was found that to achieve a completely fine microstructure with a thickness greater than 70 mm (the critical thickness), water spray should be done in several directions.

**Keywords** Ablation casting · Near-eutectic Al-Si alloy · Solidification time · Cooling rate

## Introduction

Flemings describe heat transfer in casting in which several cases of resistance delay heat transfer. These cases include liquid, solidified metal, metal–mold interface, and mold and its surroundings [1]. In many casting methods, heat transfer is controlled by the metal–mold interface, known as “Air gap.” Air gap is formed between the mold wall and the solid skin through the contraction of casting away from the mold and the expansion of the mold [2]. In order to increase the cooling rate of the melt, the air gap must be removed. One

of the inexpensive methods of removing the air gap is “ablation casting process.” In this process, a water-soluble binder is used in molding materials. Following the molten alloy pouring step and formation of solid skin around the casting, the water spray process begins on the sand mold surface and the binder gradually dissolves in water. Finally, the sand mold erodes with water and the air gap is removed. Therefore, water droplets come in direct contact with the casting surface. Thus, the cooling rate increases and eventually, the microstructure changes [2–6]. Ablation casting is an environmentally friendly and inexpensive process. Murat Tiryakoglu et al. determined the relatively good fatigue properties for the wrought alloy (6061) after ablation casting. In other words, the 6000 and 7000 series alloys can be castable using this new casting method [2, 4].

There are two approaches to the transformation of the microstructure of the as-cast component (modification of the interdendritic phases and grain refinement) in Al-Si system alloys that can promote the mechanical properties. The first approach is to use elements such as Sr, B, Y, Eu, Bi, Sb, Co, Mg, etc., in Al-Si system alloys [7–25]. Some of these elements have been used as modifiers of eutectic silicon, while

✉ Seyed Mohammad Ali Boutorabi  
boutorabi@iust.ac.ir

<sup>1</sup> Casting Research Center, School of Metallurgy and Materials Engineering, Iran University of Science and Technology, IUST, P.O. Box: 16846, Narmak, Tehran, Iran

<sup>2</sup> Center of Excellence for High Strength Alloys Technology (CEHSAT), School of Metallurgy and Materials Engineering, Iran University of Science and Technology (IUST), P.O. Box: 16846, Narmak, Tehran, Iran

the others are the refiner of  $\alpha$ -aluminum grains. Therefore, none of them apply two processes simultaneously (modification and refinement). The second approach to modifying and refining the microstructure simultaneously is to increase the cooling rate of the melt using different methods. Many researchers have studied the effect of the cooling rate of Al-Si alloys [14, 18–21, 24–32]. Some of them have evaluated the effect of the microstructure on the mechanical properties of aluminum alloys [8, 27, 33]. However, increasing the cooling rate results in a decrease in the SDAS and intermetallic compounds and improves eutectic silicon modification at the same time [8, 9, 14]. Furthermore, increasing the cooling rate leads to the soundness of the casting [1–5]. In other words, upon increasing the cooling rate, the size and number of casting defects such as shrinkage porosities, gas porosities, and the bi-films would decrease. Therefore, the cooling rate is the most essential parameter that not only controls final solidification microstructure but also decreases the casting defects, both of which lead to the promotion of the mechanical properties [2–4].

The thermal analysis technique is employed to measure the solidification characteristics during the solidification process of the molten alloy. Temperature–time curve can be extracted through data collection and the solidification characteristics such as the cooling rate, liquidus and solidus temperatures, solidification time can be determined using the first and second derivatives of the curves [26]. The results of the thermal analysis technique and metallography are finally compared, and the solidification path of the alloys is evaluated.

Aluminum–silicon casting alloys and their composites are widely used in the aerospace, automobile and military industries due to their excellent casting properties, good corrosion resistance and good weldability [13]. The microstructure of these alloys comprises  $\alpha$ -aluminum dendrites,  $\alpha$ -aluminum and silicon eutectic, primary silicon and some other compounds. The morphology and size of these phases play essential roles in the final mechanical properties of the casting. In the present study, the effects of water spray time duration and casting thickness in the ablation casting of a near-eutectic Al-Si alloy on the microstructural parameters, such as the SDAS, were investigated.

## Experimental

The designed pattern for this study is given in Fig. 1. This sloping pattern was selected to investigate the effect of the ablation process on the depth of casting with different thickness values. In the molding stage and conventional sand-casting process, the mold was produced from silica sand and sodium silicate binder; however, in the ablation process, the cope was made of silica sand and water-soluble binder and

the rest of the constituents were the same as those of the conventional sand casting.

In order to implement the thermal analysis process, eight k-type thermocouples were employed. The location of each thermocouple is shown in Fig. 1. To investigate the surface and bottom temperatures of the casting during the ablation process, a number of locations were selected. In addition, 30, 50, 70 and 90 mm thicknesses were selected. These thermocouples were connected to a high-speed data acquisition system.

Near-eutectic Al-Si alloy with the composition shown in Table 1 was melted in a resistant melting furnace at 750°C. Then, the melt was poured into the sand mold at 720°C, while the thermocouples were employed to set up the data. This process is referred to as conventional sand casting (SC).

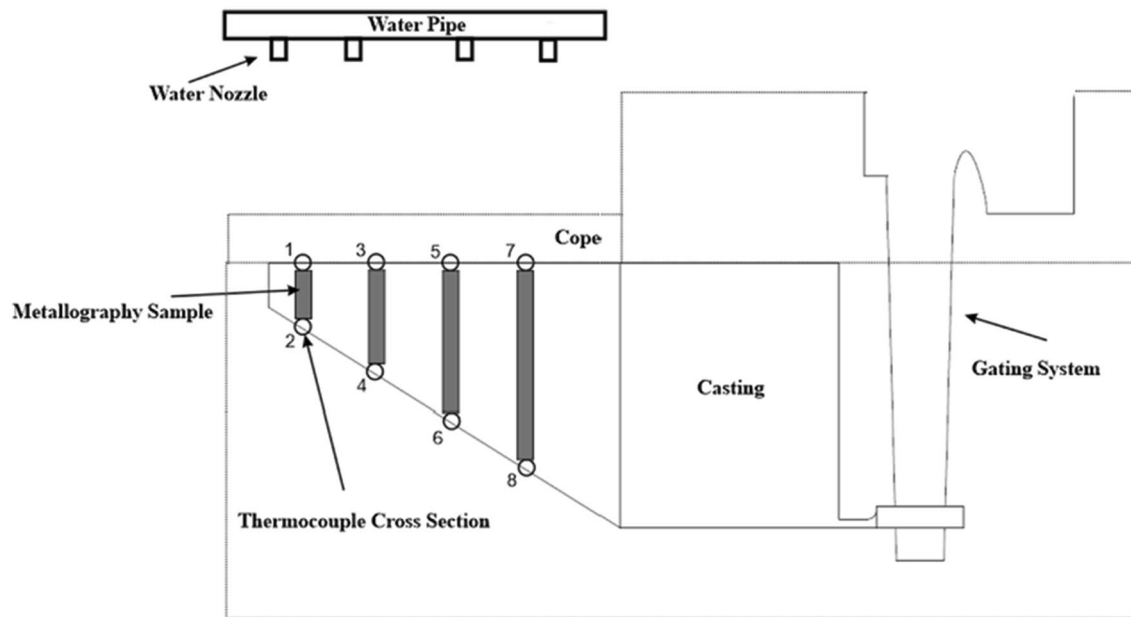
The ablation process was implemented after 100 (AB1) and 150 (AB2) seconds from the beginning of pouring the melt into the mold.

In order to evaluate the effect of the ablation process on the depth of casting with different thicknesses, the cast microstructure from surface to bottom in the locations between two thermocouples with the same thicknesses was observed. To this end, metallography samples were derived from the space between two thermocouples with the same thicknesses and each of metallography samples was divided into four equal parts from surface to bottom of the casting; moreover, the microstructure was evaluated accordingly. Elaboration of the metallography samples is given in Fig. 1 and Table 2. For example, the sample SC-30-1 is the first part from surface to bottom of SC with a thickness of 30 mm, and after that, samples SC-30-2, SC-30-3 and SC-30-4 ensue, orderly.

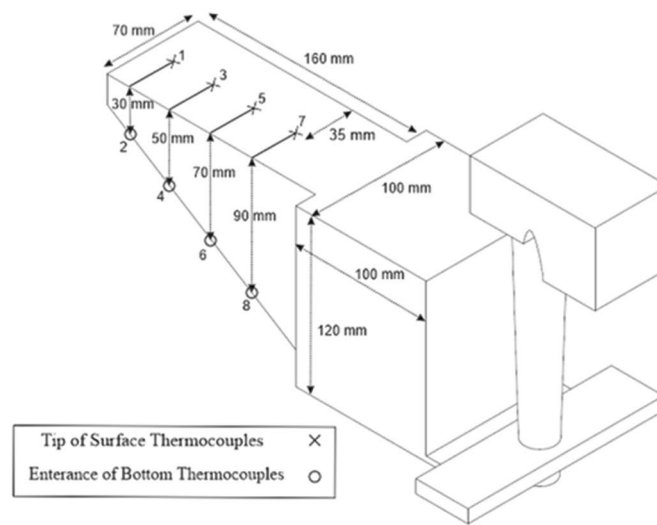
## Results and Discussion

### Thermal Analysis Data Evaluation

With the first derivative curve (the cooling rate curve), the solidification characteristics acquired from each thermocouple were determined, an example of which is given in Fig. 2. Figures 3, 4, 5 and 6 show the temperature–time curves (the cooling curve) of SC, AB1 and AB2 melts. The thermocouples located on the surface of the castings with a thickness of 30 mm were compared (SC-30-1, AB1-30-1 and AB2-30-1 thermocouples). Moreover, the solidification characteristics of each thermocouple are given in Tables 3, 4, 5 and 6. As can be seen, the  $\alpha$ -aluminum nucleation temperature ( $T_{N,\alpha}$ ), solidification end temperature ( $T_{\text{end}}$ ), eutectic temperature ( $T_{\text{eu}}$ ), solidification range ( $\Delta T = T_{N,\alpha} - T_{\text{end}}$ ) and total solidification time of each thermocouple have relatively close values. Bohlooli et al. [5] demonstrated that the ablation casting of A356 alloy did not significantly change the critical



a



b

**Fig. 1** (a) The location of metallography samples and thermocouples, (b) the dimensions of casting and exact location of thermocouples

**Table 1** Chemical composition of near-eutectic Al-Si

Element	Al	Si	Fe	Cu	Mn	Mg	Zn	Cr	Ti
Wt.%	87.62	10.50	0.48	0.52	0.06	0.26	0.44	0.01	0.11

temperatures in the thermal analysis, compared to sand casting. However, the solidification time ( $\Delta t = t_{\text{end}} - t_{N,\alpha}$ ) for all thermocouples is not the same. For this reason, the cooling

rate ( $dT/dt$ ) of each thermocouple varies. The solidification time for AB1 and AB2 samples is much shorter than that for the SC sample in all cases. According to these two items

**Table 2** The names and order of the metallography samples

90 mm	70 mm	50 mm	30 mm	Sample
SC-90-1	SC-70-1	SC-50-1	SC-30-1	SC
SC-90-2	SC-70-2	SC-50-2	SC-30-2	
SC-90-3	SC-70-3	SC-50-3	SC-30-3	
SC-90-4	SC-70-4	SC-50-4	SC-30-4	
AB1-90-1	AB1-70-1	AB1-50-1	AB1-30-1	AB1
AB1-90-2	AB1-70-2	AB1-50-2	AB1-30-2	
AB1-90-3	AB1-70-3	AB1-50-3	AB1-30-3	
AB1-90-4	AB1-70-4	AB1-50-4	AB1-30-4	
AB2-90-1	AB2-70-1	AB2-50-1	AB2-30-1	AB2
AB2-90-2	AB2-70-2	AB2-50-2	AB2-30-2	
AB2-90-3	AB2-70-3	AB2-50-3	AB2-30-3	
AB2-90-4	AB2-70-4	AB2-50-4	AB2-30-4	

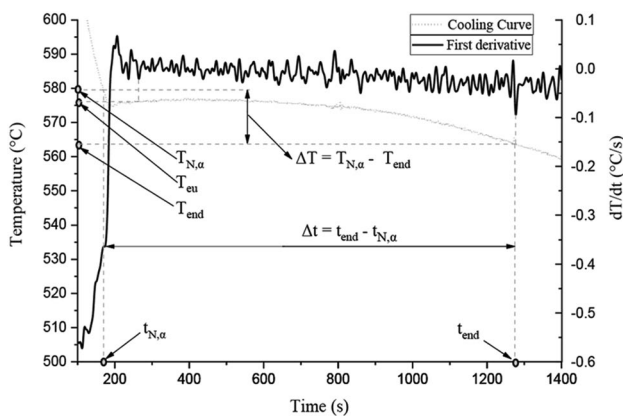


**Fig. 2** The solidification characteristic parameters of SC-50-4 thermocouple

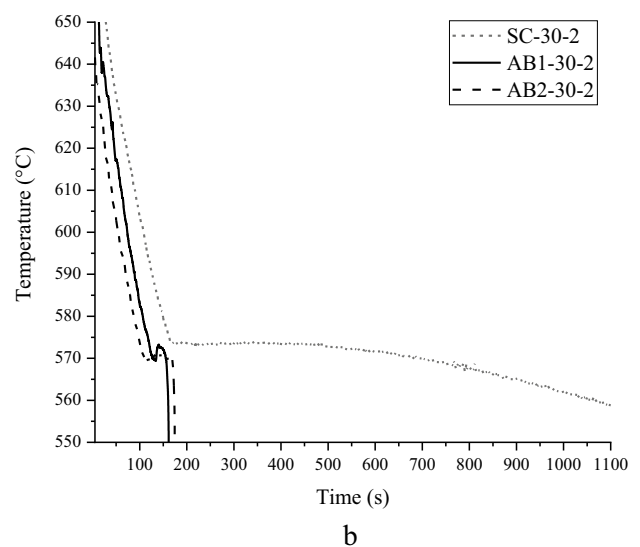
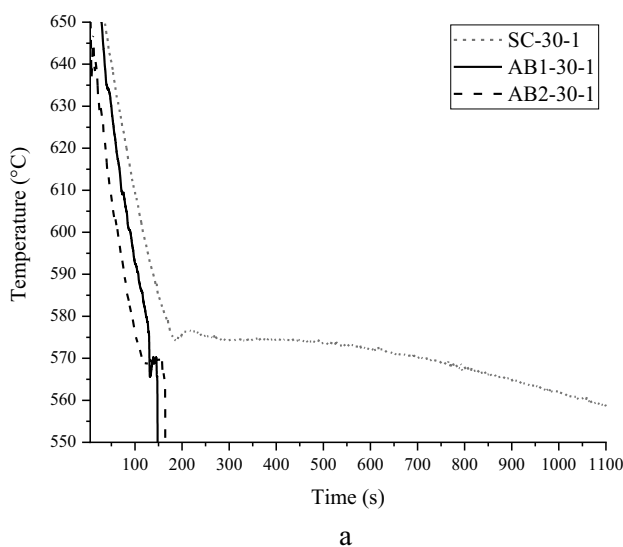


**Fig. 3** Cooling curve of (a) SC-30-1, AB1-30-1 and AB2-30-1, (b) SC-30-2, AB1-30-2 and AB2-30-2 thermocouples

(the solidification time and cooling rate), the ablated samples are expected to have a finer microstructure compared to SC. Bohlooli et al. [5] and Taghipourian et al. [3] reported that the application of ablation casting would shorten the solidification time. In addition, as a result of further water spray delay in AB2, the solidification time for all thermocouples in AB2 casting remains longer than that in AB1 casting in the same locations. In any thicknesses of AB1 and AB2 castings, the solidification time of the casting surface is shorter than that of the casting bottom in each thickness, mainly because the water sprayed on the surface of the castings makes the surface solidify sooner than that at the bottom of the castings. Besides, the air gap thickness between the solid skin and mold wall in AB2 casting is greater than that in AB1 casting because of more delay in water spray time in AB2. This phenomenon also shortens the solidification time.

The most essential parameter in the thermal analysis of the casting is “cooling rate.” This parameter shows the heat flow rate of the casting during the solidification. Therefore, the slope of the cooling curve becomes more critical. Of course, this parameter depends on some agents such as alloy type, pouring temperature, casting modulus, mold type and cooling conditions such as the amount of air gap. However, this study compared the calculated cooling rates of SC, AB1 and AB2 samples with each other, and in each ablated sample, the cooling rate of the surface was compared with that of the bottom. In this regard, Fig. 7a, b shows that the cooling rates of surface thermocouples are higher than those of bottom thermocouples corresponding to those in AB1 and AB2 castings. According to Fig. 7a, the cooling rates of surface thermocouples do not differ significantly from each other in AB1 and AB2 castings; however, the cooling rates of surface thermocouples of the AB1 sample are higher than those of SC and AB2 castings due to the shorter water spray

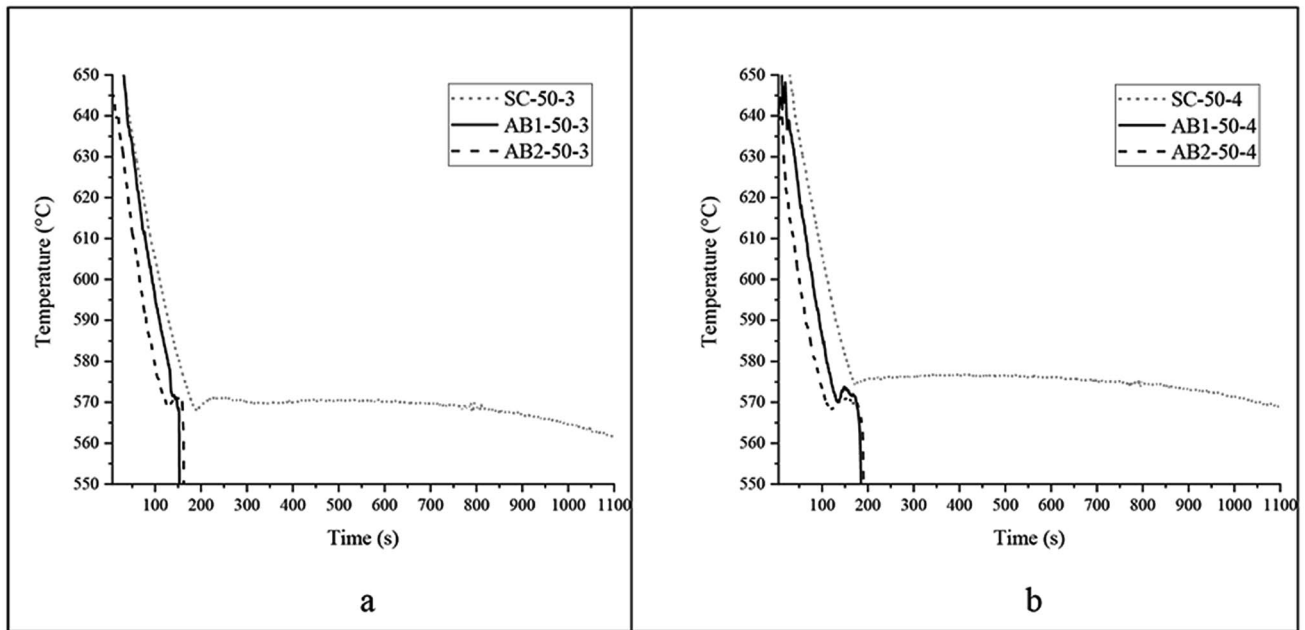


**Fig. 4** Cooling curve of (a) SC-50-3, AB1-50-3 and AB2-50-3, (b) SC-50-4, AB1-50-4 and AB2-50-4 thermocouples

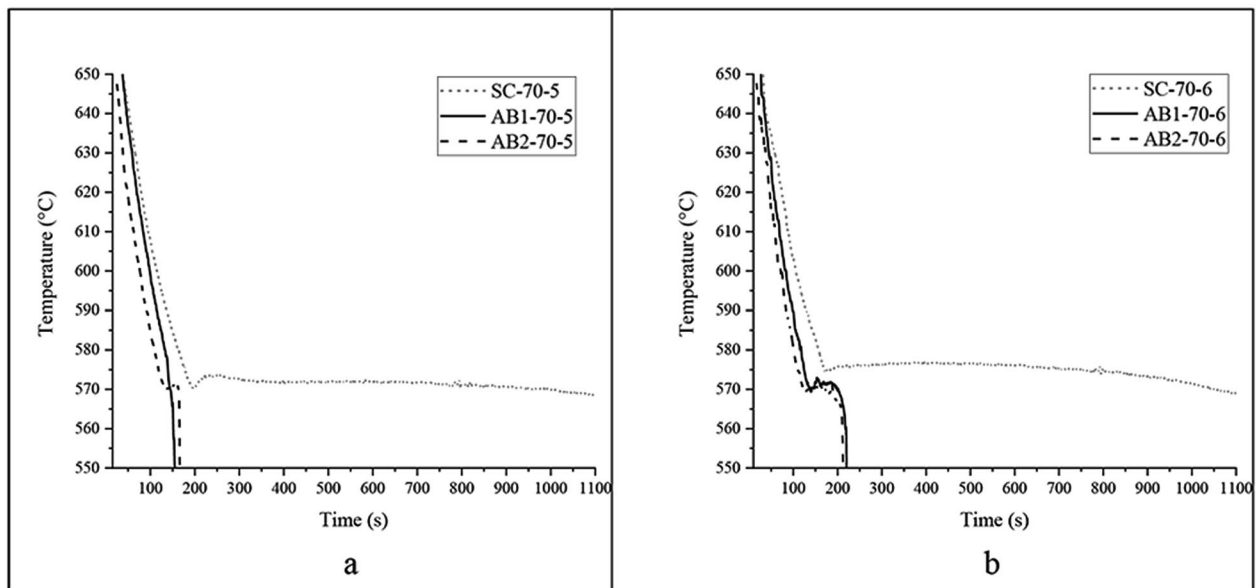


**Fig. 5** Cooling curve of (a) SC-70-5, AB1-70-5 and AB2-70-5, (b) SC-70-6, AB1-70-6 and AB2-70-6 thermocouples

time after pouring and lower thickness of air gap formed before water spray.

According to Fig. 7b, upon increasing the thickness of the casting, the cooling rate at the bottom of the casting decreases, mainly because the distance from the water spray nozzle increases. Nevertheless, the cooling rate of the ablated castings is higher than that of SC at the bottom; however, the cooling rates of AB1 and AB2 are not much

different. However, the cooling rates of surface thermocouples are 6.9–43.6 times for AB1 and 4.8–22.8 times for AB2, compared to SC. In the following, the cooling rates of the bottom thermocouples are 1.5–21.9 times for AB1 and 1.3–19.9 times for AB2 compared to SC in different thicknesses. Campbell et al. pointed out that in case the water spray time and method were appropriate, the cooling rate could be achieved at 100°C/s in the ablation casting process

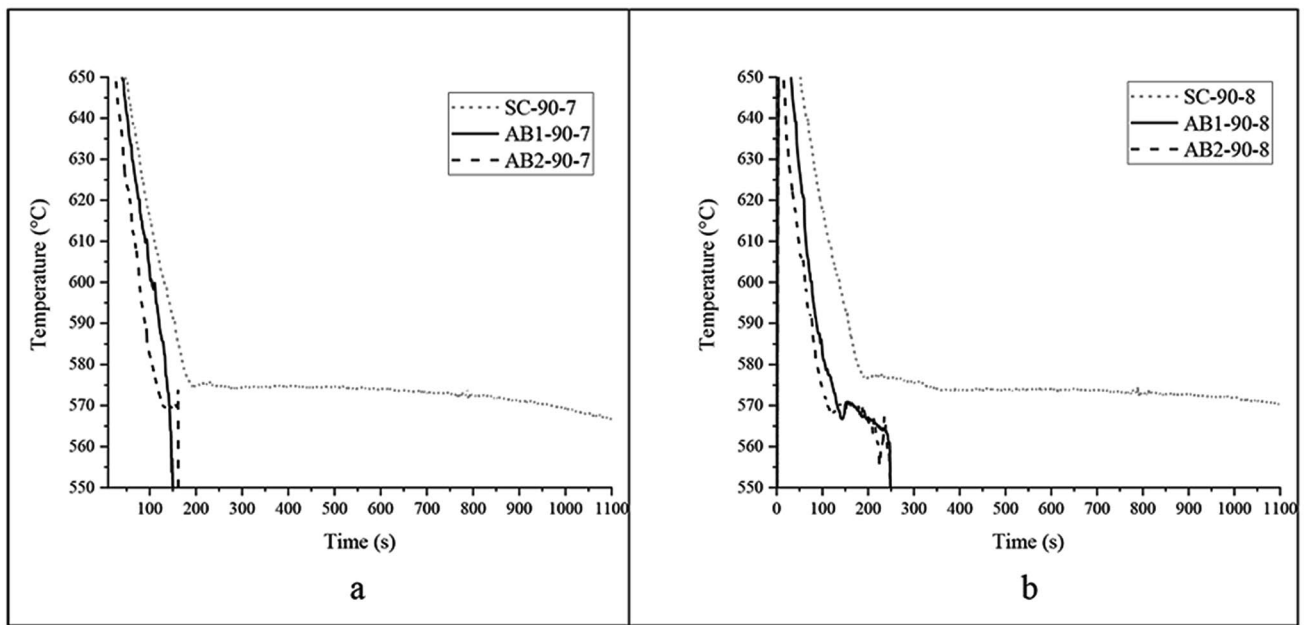


**Fig. 6** Cooling curve of (a) SC-90-7, AB1-90-7 and AB2-90-7, (b) SC-90-8, AB1-90-8 and AB2-90-8 thermocouples

**Table 3** The solidification characteristics of SC-30-1, AB1-30-1, AB2-30-1, SC-30-2, AB1-30-2 and AB2-30-2 thermocouples

	SC-30-1	AB1-30-1	AB2-30-1	SC-30-2	AB1-30-2	AB2-30-2
$T_{N,\alpha}$ (°C)	580	578	580	581	583	580
$T_{eu}$ (°C)	575	570	569	572	570	572
$T_{end}$ (°C)	563	562	566	563	568	567
$\Delta T$ (°C)	17	16	14	18	15	13
$\Delta t$ (s)	917	18	70	937	52	79
$dT/dt$ (°C/s)	0.096	0.660	0.461	0.068	0.393	0.416

**Table 4** The solidification characteristics of SC-50-3, AB1-50-3, AB2-50-3, SC-50-4, AB1-50-4 and AB2-50-4 thermocouples

	SC-50-3	AB1-50-3	AB2-50-3	SC-50-4	AB1-50-4	AB2-50-4
$T_{N,\alpha}$ (°C)	583	582	582	578	578	577
$T_{eu}$ (°C)	573	571	570	575	572	570
$T_S$ (°C)	564	567	566	563	565	563
$\Delta T$ (°C)	19	15	16	15	13	14
$\Delta t$ (s)	896	23	65	1104	67	90
$dT/dt$ (°C/s)	0.063	0.887	0.418	0.025	0.196	0.338

**Table 5** The solidification characteristics of SC-70-5, AB1-70-5, AB2-70-5, SC-70-6, AB1-70-6 and AB2-70-6 thermocouples

	SC-70-5	AB1-70-5	AB2-70-5	SC-70-6	AB1-70-6	AB2-70-6
$T_{N,\alpha}$ (°C)	578	579	578	578	580	578
$T_{eu}$ (°C)	574	572	570	575	571	570
$T_S$ (°C)	563	567	566	564	563	564
$\Delta T$ (°C)	15	12	12	14	17	14
$\Delta t$ (s)	1085	14	54	1099	102	99
$dT/dt$ (°C/s)	0.020	0.872	0.456	0.015	0.329	0.298

**Table 6** The solidification characteristics of SC-90-7, AB1-90-7, AB2-90-7, SC-90-8, AB1-90-8 and AB2-90-8 thermocouples

	SC-90-7	AB1-90-7	AB2-90-7	SC-90-8	AB1-90-8	AB2-90-8
$T_{N,\alpha}$ (°C)	583	581	578	580	578	578
$T_{eu}$ (°C)	575	572	570	575	570	571
$T_s$ (°C)	563	564	567	564	567	560
$\Delta T$ (°C)	20	17	11	16	11	18
$\Delta t$ (s)	1092	10	54	1088	114	142
$dT/dt$ (°C/s)	0.066	0.856	0.432	0.061	0.092	0.078

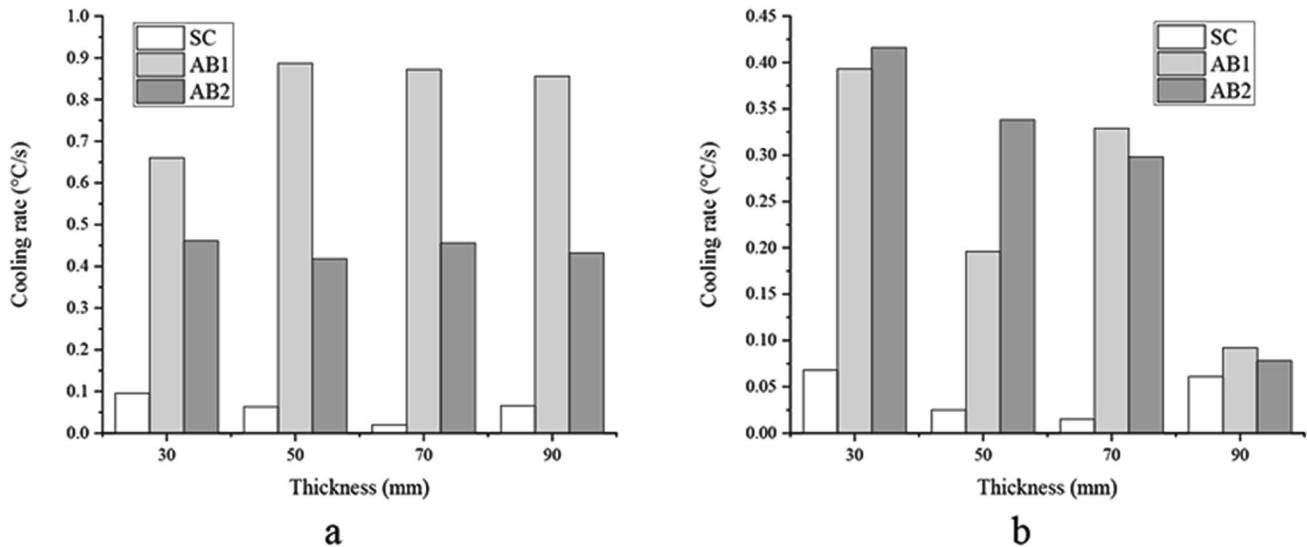


**Fig. 7** The cooling rate of (a) surface and (b) bottom thermocouples at 30, 50, 70 and 90 mm thicknesses for SC, AB1 and AB2 castings

[2]. Although the cooling rate in this study was less than 1 °C/s in the AB1 and AB2 castings, a relatively fine microstructure was obtained, even at the bottom.

## Microstructural Evaluations

### Microscopic Observations

Figures 8, 9, 10 and 11 show the microstructures of SC, AB1 and AB2 melts, respectively. As mentioned earlier, in the case of each thickness, the metallography samples were cut into four equal parts from the surface to the bottom, and the corresponding samples in different melts were compared with each other. As shown, upon applying water spray on the surface of the casting, a remarkable transformation took place in the microstructure of the aluminum alloy. The morphology of the silicon phase changed from the coarse needle-like morphology in SC to fine needle-like or fibrous in both AB1 and AB2. In the microstructure of the ablated samples, primary  $\alpha$ -aluminum and eutectic  $\alpha$ -aluminum are separable; however, in the SC sample, this is not the case. Campbell [2] achieved very fine eutectic silicon in the ablation casting of A356 alloy (less than 1  $\mu$ m). A very fine

eutectic in many microstructural spots of AB1 and AB2 castings was observed, similar to the one presented in Fig. 12.

The primary  $\alpha$ -aluminum phase in SC was equiaxed; however, in AB1 and AB2, a mixture of the columnar and equiaxed structures of  $\alpha$ -aluminum was observed. With greater precision of the microscopic images, it can be observed that in some locations of ablated castings such as AB1-50-2, AB2-50-2, AB1-70-2 and AB2-70-2, the metallography samples throughout the microstructure are characterized by a very fine structure at both primary  $\alpha$ -aluminum and eutectic phases. It is suggested in the following that AB1-30-1 and AB2-30-1 (close to the surface) have some relatively coarse eutectic silicon as a result of nucleation of eutectic silicon before the start of water spray. Liao et al. reported that quenching of solidifying near-eutectic Al-Si casting alloy led to the formation of a mixture of a rather coarse eutectic and a very fine eutectic. This phenomenon was observed in some microstructures such as AB1-30-1 and AB2-30-1. Moreover, it was observed that upon moving away from the surface to the bottom in AB1 and AB2 castings, the primary  $\alpha$ -aluminum and eutectic silicon became relatively coarse (see AB1-70-4, AB2-70-4, AB1-90-4 and AB2-90-4 microstructures). These results demonstrated that



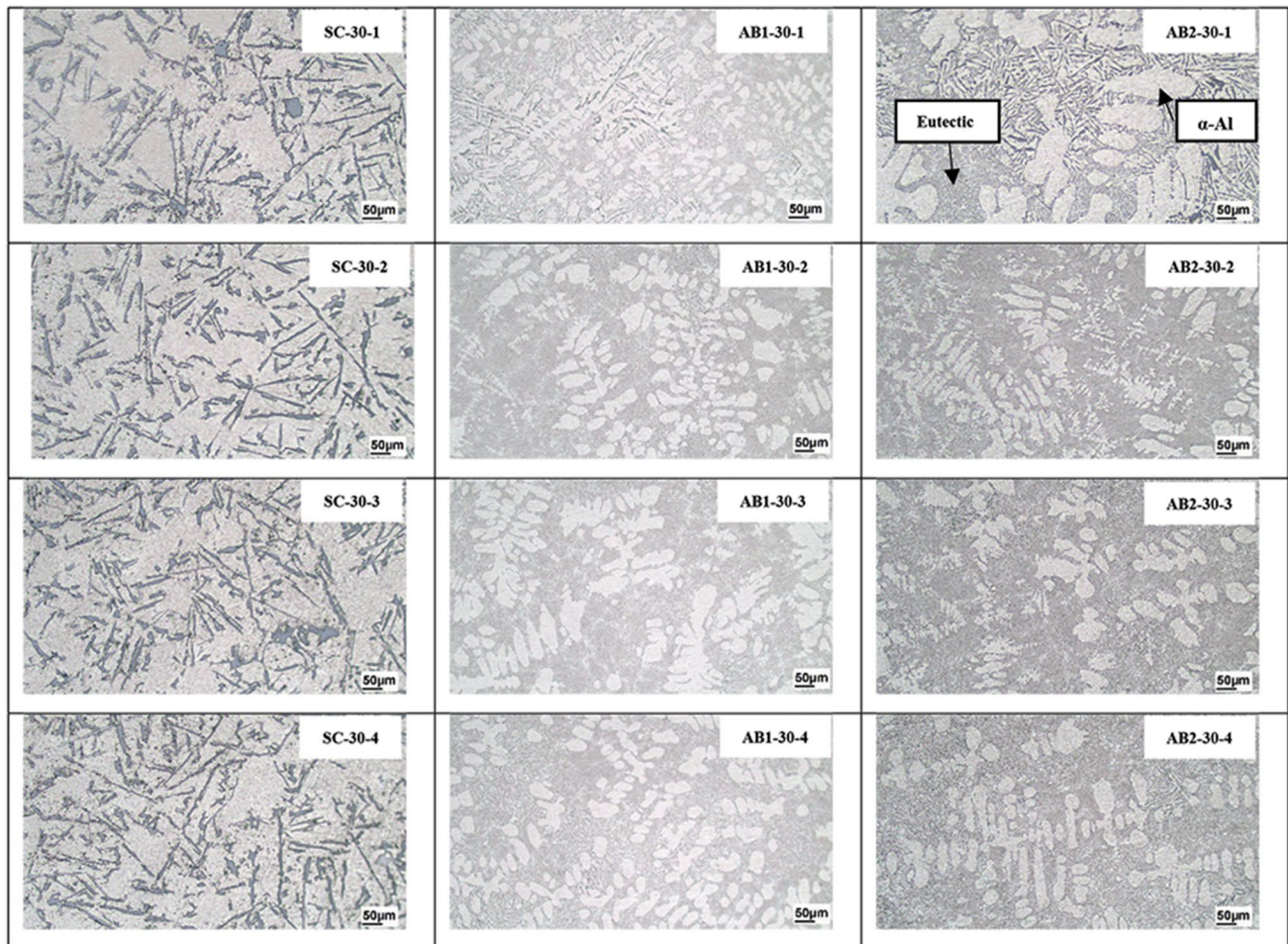


**Fig. 8** The microstructure of SC, AB1 and AB2 castings at 30 mm thickness

increasing the sample thickness (more than 70 mm) attenuated the effect of the ablation process at the bottom of the casting; consequently, thickness 70 mm is essential to the ablation process and a suitable water spray system must be designed to cover all casting surfaces in the case of the thickness above 70 mm.

### Calculated SDAS

Figures 13, 14, 15 and 16 show the SDAS in the case of different melts and thicknesses. With the application of the water spray process, the SDAS was reduced, compared to SC. Hence, the decrement rates for SDAS compared to SC at different thicknesses in the first, second, third and fourth quarters of metallography samples are 56.8–88.6% and

61.4–86.1%, 74.1–87.3% and 68.5–90.1%, 71.8–75.7% and 57.9–70.6%, and 56.4–77.8% and 38.1–59.7% for AB1 and AB2 castings, respectively. As observed earlier, the maximum decrement of SDAS belongs to the second quarter of AB1 and AB2 casting microstructures. In the previous studies on the ablation casting process of aluminum alloys, the lowest amounts of the SDAS were 25.5  $\mu\text{m}$  [3] and 35  $\mu\text{m}$  [5] for A356 alloy; however, in this study, the SDAS was about 8  $\mu\text{m}$  in several locations of ablated metallography samples. Nevertheless, the exact location of metallography samples has not been mentioned in any of the previous researches, a flaw that this study attempted to resolve. Due to the differences among such parameters such as alloy type, casting modulus and water spray time in different studies, comparing the reported data does not seem very logical.



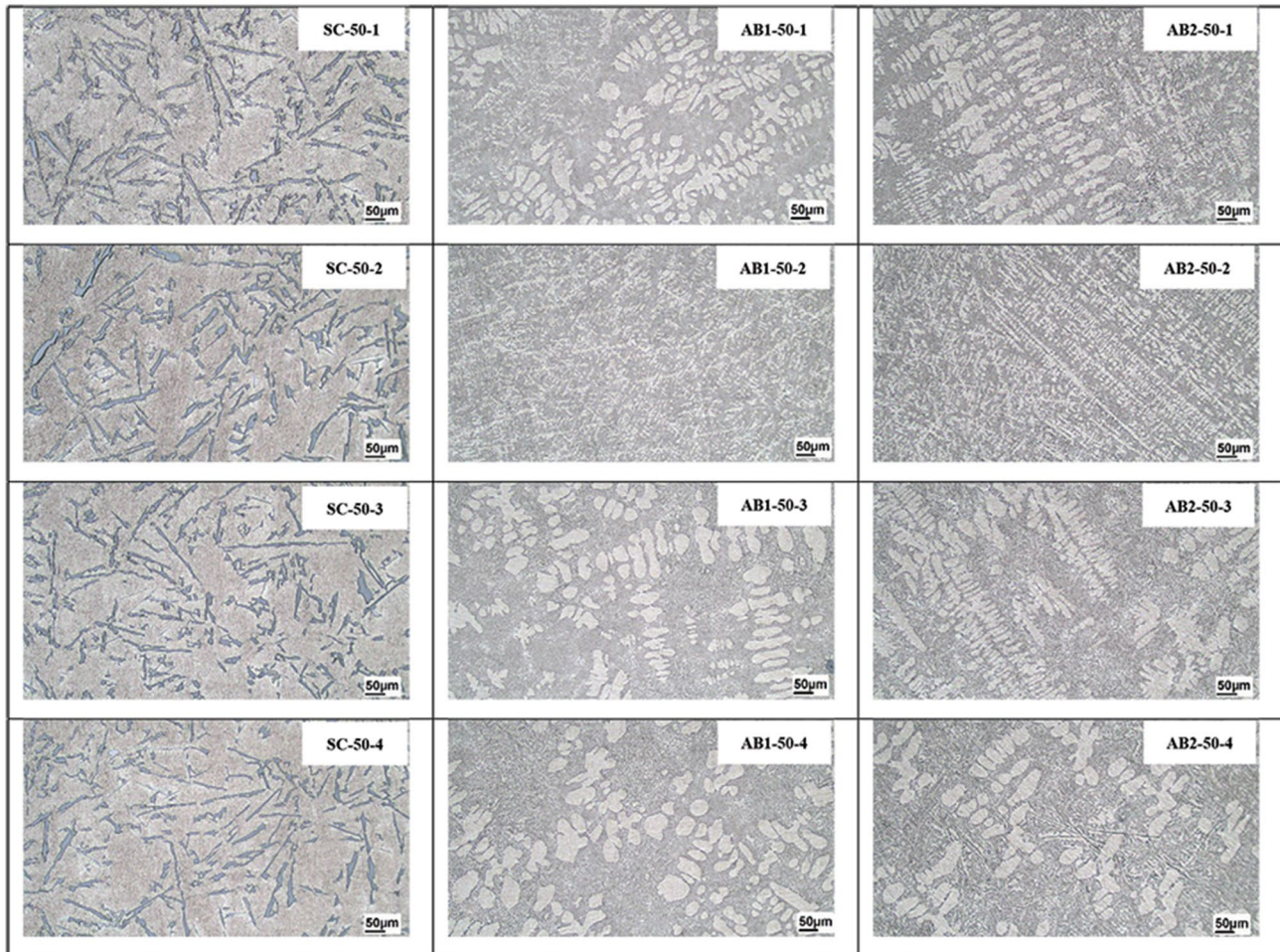


**Fig. 9** The microstructure of SC, AB1 and AB2 castings at 50 mm thickness

The most crucial parameter associated with the ablation casting process is the water spray start time to achieve the finest microstructure and the best mechanical properties [2]. In this study, the water spray start times were selected as 100 s (AB1) and 150 s (AB2) after pouring the molten alloy. Before water spray, the solidification process in different casting locations has begun, especially on the wall mold, toward the lower thickness of the casting. This phenomenon occurs at 150 s to a greater extent than that at 100 s after pouring melt. However, according to the thermal analysis and microstructure, the results of AB1 and AB2 castings were not much different, especially at the bottom and center of castings. Being a modified eutectic silicon among the

majority of the microstructures of AB1 and AB2 castings, the Al-Si eutectic reaction did not occur right at the water spray moment. However, the primary  $\alpha$ -aluminum nucleated and grew a little, especially in AB2 casting. Of course, it appears that the whole alloy was completely molten in some locations such as AB1-50-2 and AB2-50-2 metallography samples. Nevertheless, according to the argument of Campbell et al., if water spray begins on time, the fine SDAS will be achievable [2]. In addition, they suggested that the role of the SDAS was less significant than that of the eutectic in the mechanical properties, and even if the water spray occurred before the eutectic reaction, the relatively desired properties could still be achieved [2].



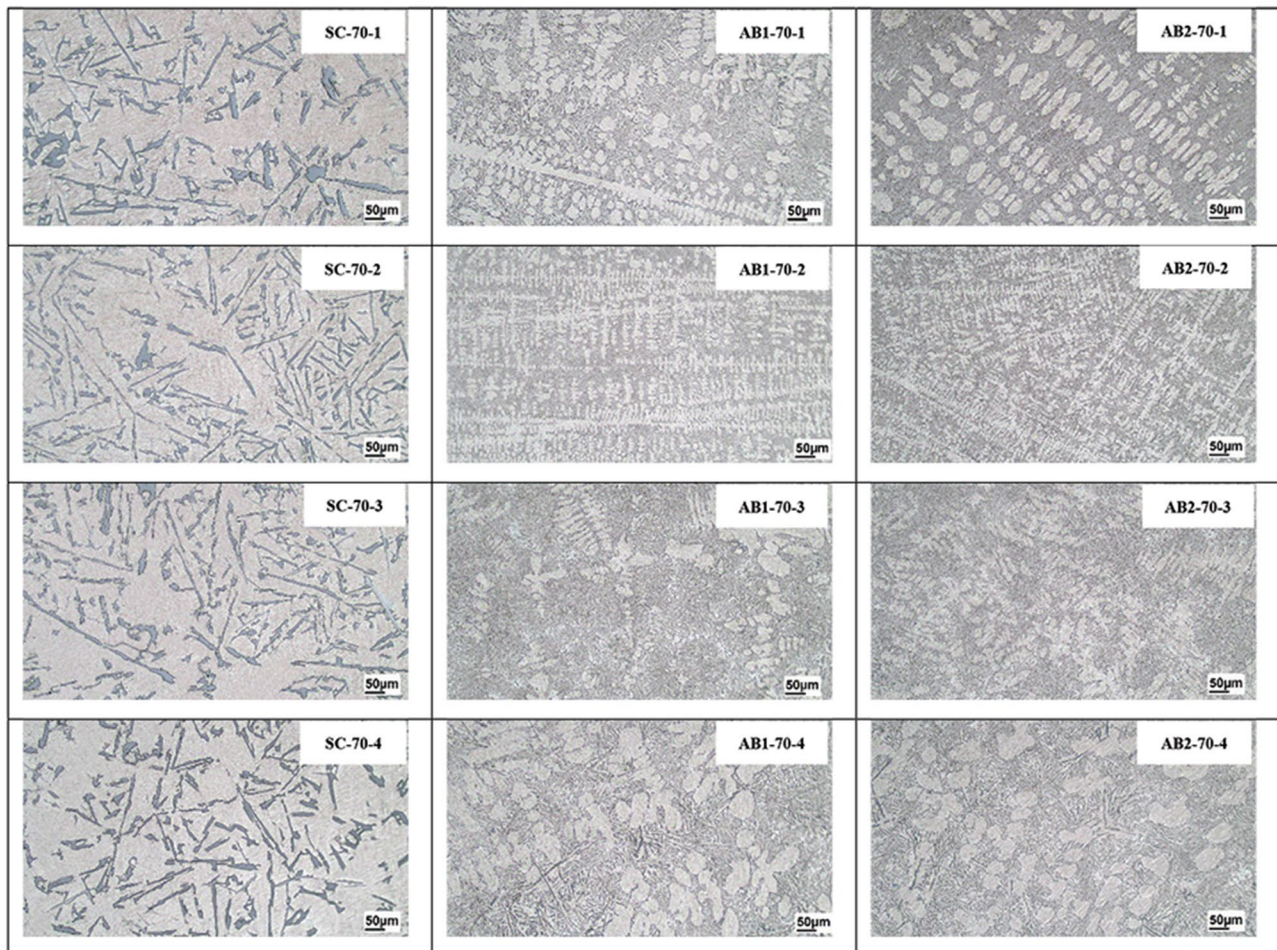


Fig. 10 The microstructure of SC, AB1 and AB2 castings at 70 mm thickness

## Conclusion

In this study, a sloping casting was prepared using conventional sand casting and ablation casting processes (with two water spray times of 100 and 150 s), and the following results were obtained:

- Ablation casting did not significantly change  $\alpha$ -aluminum nucleation temperature, solidification end temperature, and eutectic temperature in the thermal analysis.
- Application of water spray on the surface of the casting (ablation casting) shortened the solidification time and increased the cooling rate compared to conventional sand casting. The cooling rate of surface thermocouples was 6.9–43.6 times for AB1 and 4.8–22.8 times for AB2 compared to SC. Moreover, the cooling rates of the bottom thermocouples were 1.5–21.9 times for AB1 and 1.3–19.9 times for AB2 compared to SC with different thicknesses.
- The faster water spray in the ablation casting (100 s rather than 150 s) did not significantly change the cooling rate and SDAS.
- Although the cooling rate was less than  $1^{\circ}\text{C/s}$  in the AB1 and AB2 castings, eutectic silicon with a size of about  $1\ \mu\text{m}$  was obtained and the SDAS was  $8\ \mu\text{m}$ , especially at the center of the ablated castings.
- The decrement rates of SDAS compared to SC at different thicknesses in the first, second, third and fourth quarters of metallography samples were 56.8–88.6% and 61.4–86.1%, 74.1–87.3% and 68.5–90.1%, 71.8–75.7% and 57.9–70.6%, and 56.4–77.8% and 38.1–59.7% for AB1 and AB2 castings, respectively.
- According to the microstructure images and the calculated SDAS, upon increasing the casting thickness from 30 to 90 mm, the effect of the water spray at a depth of casting was attenuated due to increase in the casting thickness. Therefore, thickness 70 mm is essential to the ablation process and a suitable water spray system must be designed to cover all casting surfaces for the thickness above 70 mm.



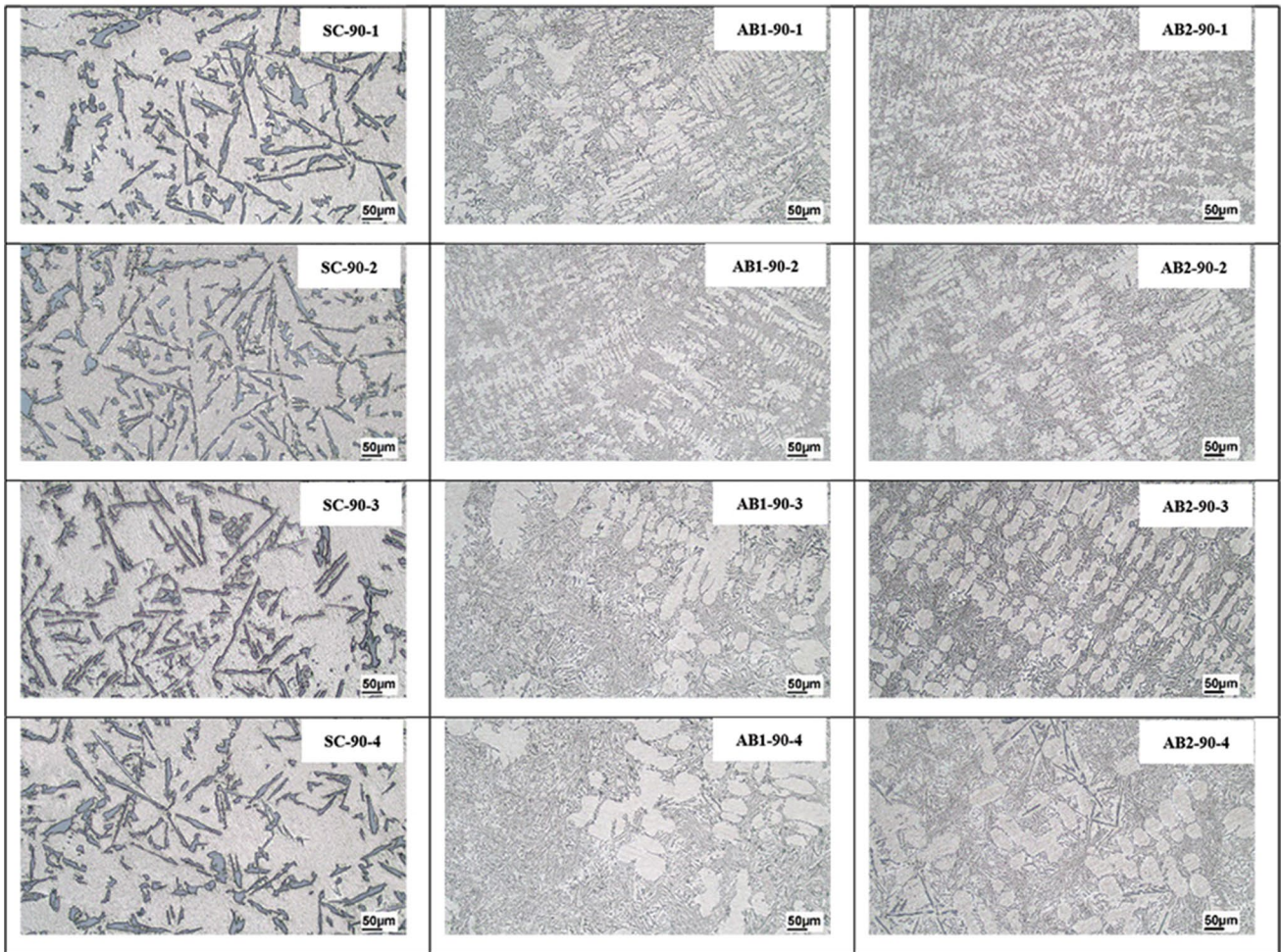


Fig. 11 The microstructure of SC, AB1 and AB2 castings at 90 mm thickness

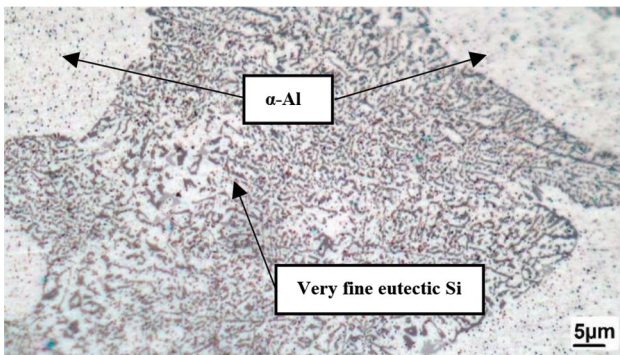


Fig. 12 Very fine Si eutectic in AB1-30-1 metallography sample

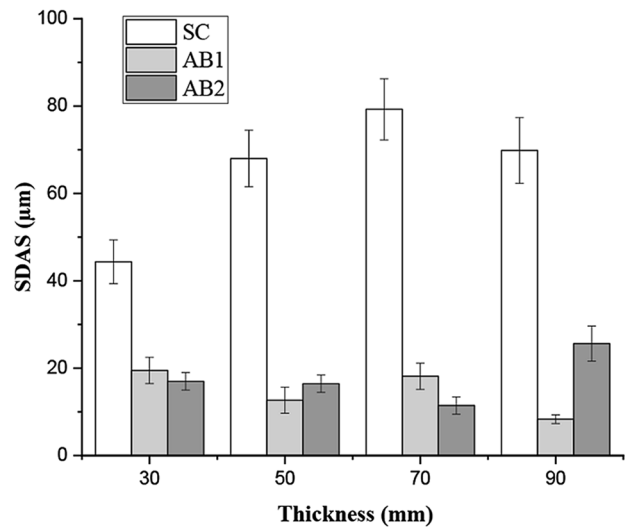
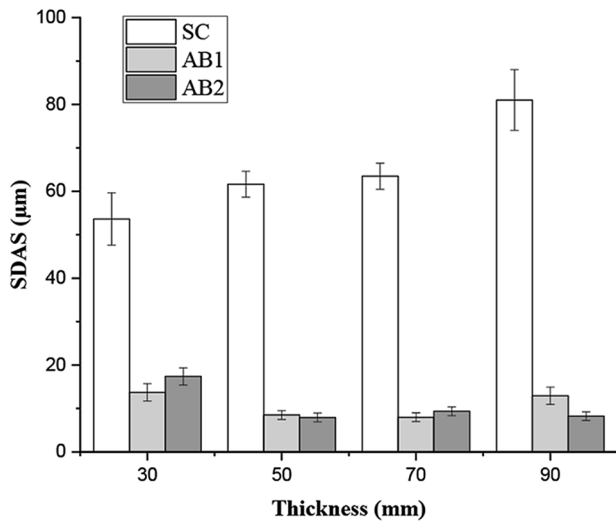
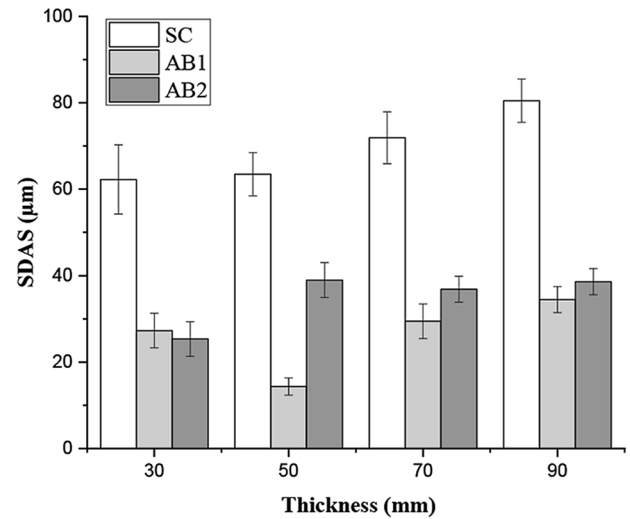


Fig. 13 The calculated SDAS of first quarter of metallography samples of SC, AB1 and AB2 castings at 30, 50, 70 and 90 mm thicknesses



**Fig. 14** The calculated SDAS of second quarter of metallography samples of SC, AB1 and AB2 castings at 30, 50, 70 and 90 mm thicknesses



**Fig. 16** The calculated SDAS of fourth quarter of metallography samples of SC, AB1 and AB2 castings at 30, 50, 70 and 90 mm thicknesses

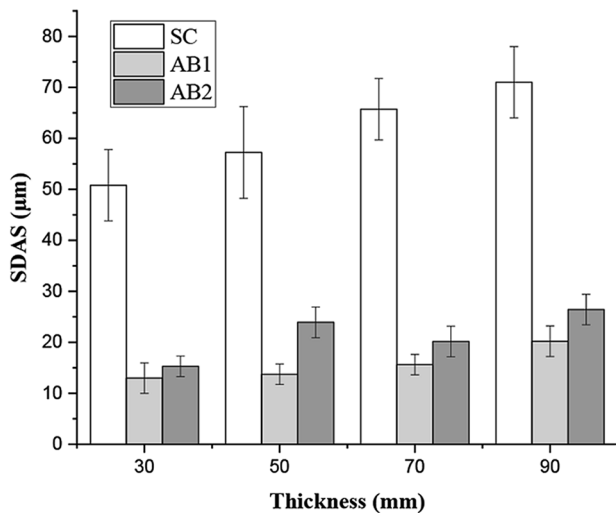


**Fig. 15** The calculated SDAS of third quarter of metallography samples of SC, AB1 and AB2 castings at 30, 50, 70 and 90 mm thicknesses

## References

1. M.C. Flemings, Solidification processing. *Metall. Trans.* **5**(10), 2121–2134 (1974)
2. J. Grassi, J. Campbell, M. Hartlieb, J. Major, Ablation casting, aluminum alloys: fabrication, characterization and applications. TMS (2008)
3. M. Taghipourian, M. Mohammadaliha, S. Boutorabi, S. Mirdamadi, The effect of waterjet beginning time on the microstructure and mechanical properties of A356 aluminum alloy during the ablation casting process. *J. Mater. Process. Technol.* **238**, 89–95 (2016)
4. M. Tiryakioglu, P. Eason, J. Campbell, Fatigue life of ablation cast 6061-t6 components. In: 13th International Conference on Aluminum Alloys (ICAA 13): Conference Proceedings, Springer, 2017, p. 491.
5. V. Bohlooli, M.S. Mahalli, S. Boutorabi, Effect of ablation casting on microstructure and casting properties of A356 aluminium casting alloy. *Acta Metall. Sin. (Engl. Lett.)*. **26**(1), 85–91 (2013)
6. S. Boutorabi, P. Torkaman, J. Campbell, A. Zolfaghari, Structure and properties of carbon steel cast by the ablation process. *Int. J. Metalcast.* **15**(1), 306–318 (2021)
7. R. Ahmad, M. Asmael, Influence of cerium on microstructure and solidification of eutectic Al–Si piston alloy. *Mater. Manuf. Process.* **31**(15), 1948–1957 (2016)

8. A. Samuel, H. Doty, S. Valtierra, F. Samuel, Effect of Sr-P interaction on the microstructure and tensile properties of A413. 0 type alloys *Adv. Mater. Sci. Eng.* **2016** (2016)
9. S. Shabestari, S. Ghodrat, Assessment of modification and formation of intermetallic compounds in aluminum alloy using thermal analysis. *Mater. Sci. Eng. A.* **467**(1–2), 150–158 (2007)
10. M. Mahta, M. Emamy, A. Daman, A. Keyvani, J. Campbell, Precipitation of Fe rich intermetallics in Cr-and Co-modified A413 alloy. *Int. J. Cast Met. Res.* **18**(2), 73–79 (2005)
11. A. Dahle, K. Nogita, S. McDonald, C. Dinnis, L. Lu, Eutectic modification and microstructure development in Al–Si Alloys. *Mater. Sci. Eng. A.* **413**, 243–248 (2005)
12. M. Mahmoud, A. Samuel, H. Doty, S. Valtierra, F. Samuel, Effect of rare earth metals, Sr, and Ti addition on the microstructural characterization of A413. 1 alloy. *Adv. Mater. Sci. Eng.* **2017** (2017)
13. S. Jigajinni, K. Venkateswarlu, S. Kori, Computer aided cooling curve analysis for Al-5Si and Al-11Si alloys. *Int. J. Eng. Sci. Technol.* **3**(6), 257–272 (2011)
14. S. Farahany, A. Ourdjini, M.H. Idris, S. Shabestari, Computer-aided cooling curve thermal analysis of near eutectic Al–Si–Cu–Fe alloy. *J. Therm. Anal. Calorim.* **114**(2), 705–717 (2013)
15. J. Li, X. Wang, T. Ludwig, Y. Tsunekawa, L. Arnberg, J. Jiang, P. Schumacher, Modification of eutectic Si in Al–Si alloys with Eu addition. *Acta Mater.* **84**, 153–163 (2015)
16. J. Rao, J. Zhang, R. Liu, J. Zheng, D. Yin, Modification of eutectic Si and the microstructure in an Al-7Si alloy with barium addition. *Mater. Sci. Eng. A.* **728**, 72–79 (2018)
17. P. Ma, Z. Wei, Y. Jia, Z. Yu, K.G. Prashanth, S. Yang, C. Li, L. Huang, J. Eckert, Mechanism of formation of fibrous eutectic Si and thermal conductivity of SiCp/Al-20Si composites solidified under high pressure. *J. Alloy. Compd.* **709**, 329–336 (2017)
18. L. Li, D. Li, F. Mao, J. Feng, Y. Zhang, Y. Kang, Effect of cooling rate on eutectic Si in Al-7.0 Si-0.3 Mg alloys modified by La additions. *J. Alloys Compd.* **826**, 154206 (2020)
19. S. Farahany, A. Ourdjini, M. Idarsi, S. Shabestari, Evaluation of the effect of Bi, Sb, Sr and cooling condition on eutectic phases in an Al–Si–Cu alloy (ADC12) by in situ thermal analysis. *Thermochim. Acta.* **559**, 59–68 (2013)
20. S. Valtierra, J. Lacaze, Effect of strontium and cooling rate upon eutectic temperatures of A319 aluminum alloy. *Scr. Mater.* **52**(6), 439–443 (2005)
21. H. Liao, M. Zhang, J. Bi, K. Ding, X. Xi, S. Wu, Eutectic solidification in near-eutectic Al-Si casting alloys. *J. Mater. Sci. Technol.* **26**(12), 1089–1097 (2010)
22. H. Liao, M. Zhang, Q. Wu, H. Wang, G. Sun, Refinement of eutectic grains by combined addition of strontium and boron in near-eutectic Al–Si alloys. *Scr. Mater.* **57**(12), 1121–1124 (2007)
23. O. Gursoy, G. Timelli, Lanthanides: a focused review of eutectic modification in hypoeutectic Al–Si alloys. *J. Mater. Res. Technol.* **9**(4), 8652–8666 (2020)
24. G. Mao, H. Yan, C. Zhu, Z. Wu, W. Gao, The varied mechanisms of yttrium (Y) modifying a hypoeutectic Al–Si alloy under conditions of different cooling rates. *J. Alloy Compd.* **806**, 909–916 (2019)
25. O.E. Sebaie, A. Samuel, F. Samuel, H. Doty, The effects of mischmetal, cooling rate and heat treatment on the eutectic Si particle characteristics of A319. 1, A356. 2 and A413. 1 Al-Si casting alloys. *Mater. Sci. Eng. A Struct. Mater. Prop. Microstruct. Process.* **480**(1–2), 342–355 (2008)
26. D. Emadi, L.V. Whiting, Determination of solidification characteristics of Al-Si alloys by thermal analysis. *Trans. Am. Foundry Soc.* **110**, 285–296 (2002)
27. M. Mohandass, J. Venkatesan, N. Nallusamy, Influence of cooling rate on fatigue behaviour of eutectic Al-Si (A413) alloy casting. *Appl. Mech. Mater. Trans Tech Publ.* **2015**, 490–494
28. I. Aguilera-Luna, M. Castro-Román, J. Escobedo-Bocardo, F. García-Pastor, M. Herrera-Trejo, Effect of cooling rate and Mg content on the Al–Si eutectic for Al–Si–Cu–Mg alloys. *Mater. Charact.* **95**, 211–218 (2014)
29. S. Shabestari, M. Malekan, Thermal analysis study of the effect of the cooling rate on the microstructure and solidification parameters of 319 aluminum alloy. *Can. Metall. Q.* **44**(3), 305–312 (2005)
30. L. Zhang, S. Chen, Q. Li, G. Chang, Formation mechanism and conditions of fine primary silicon being uniformly distributed on single  $\alpha$ Al matrix in Al-Si alloys. *Mater. Des.* **193**, 108853 (2020)
31. R. Kakitani, C.B. Cruz, T.S. Lima, C. Brito, A. Garcia, N. Cheung, Transient directional solidification of a eutectic Al–Si–Ni alloy: Macrostructure, microstructure, dendritic growth and hardness. *Materialia.* **7**, 100358 (2019)
32. X. Ao, H. Xia, J. Liu, Q. He, S. Lin, A numerical study of irregular eutectic in Al-Si alloys under a large undercooling. *Comput. Mater. Sci.* **186**, 110049 (2021)
33. A. Mazahery, M.O. Shabani, Modification mechanism and microstructural characteristics of eutectic Si in casting Al-Si alloys: a review on experimental and numerical studies. *Jom.* **66**(5), 726–738 (2014)

**Publisher's Note** Springer Nature remains neutral with regard to jurisdictional claims in published maps and institutional affiliations.